Computational and Structural Biotechnology Journal 18 (2020) 922–932

COMPUTATIONAL AND STRUCTURAL BIOTECHNOLOGY JOURNAL

journal homepage: www.elsevier.com/locate/csbj

Fluorescent substrates for haloalkane dehalogenases: Novel probes for mechanistic studies and protein labeling

Veronika Dockalova [a], Esther M. Sanchez-Carnerero [b], Zuzana Dunajova [a], Eduardo Palao [b], Michaela Slanska [a], Tomas Buryska [a], Jiri Damborsky [a,c], Petr Klán [b,*], Zbynek Prokop [a,c,*]

[a] Loschmidt Laboratories, Department of Experimental Biology and RECETOX, Masaryk University, Kamenice 5/A13, 625 00 Brno, Czech Republic
[b] Department of Chemistry and RECETOX, Masaryk University, Kamenice 5, 625 00 Brno, Czech Republic
[c] International Clinical Research Center, St. Anne's University Hospital, Pekarska 53, 656 91 Brno, Czech Republic

ARTICLE INFO

Article history:
Received 29 December 2019
Received in revised form 30 March 2020
Accepted 31 March 2020
Available online 8 April 2020

Keywords:
Haloalkane dehalogenase
Fluorescent substrate
Enzyme kinetics
Mechanism
Protein labeling

ABSTRACT

Haloalkane dehalogenases are enzymes that catalyze the cleavage of carbon-halogen bonds in halogenated compounds. They serve as model enzymes for studying structure–function relationships of >100.000 members of the α/β-hydrolase superfamily. Detailed kinetic analysis of their reaction is crucial for understanding the reaction mechanism and developing novel concepts in protein engineering. Fluorescent substrates, which change their fluorescence properties during a catalytic cycle, may serve as attractive molecular probes for studying the mechanism of enzyme catalysis. In this work, we present the development of the first fluorescent substrates for this enzyme family based on coumarin and BODIPY chromophores. Steady-state and pre-steady-state kinetics with two of the most active haloalkane dehalogenases, DmmA and LinB, revealed that both fluorescent substrates provided specificity constant two orders of magnitude higher (0.14–12.6 $\mu M^{-1}\ s^{-1}$) than previously reported representative substrates for the haloalkane dehalogenase family (0.00005–0.014 $\mu M^{-1}\ s^{-1}$). Stopped-flow fluorescence/FRET analysis enabled for the first time monitoring of all individual reaction steps within a single experiment: (i) substrate binding, (ii–iii) two subsequent chemical steps and (iv) product release. The newly introduced fluorescent molecules are potent probes for fast steady-state kinetic profiling. In combination with rapid mixing techniques, they provide highly valuable information about individual kinetic steps and mechanism of haloalkane dehalogenases. Additionally, these molecules offer high specificity and efficiency for protein labeling and can serve as probes for studying protein hydration and dynamics as well as potential markers for cell imaging.

1. Introduction

Haloalkane dehalogenases (EC 3.8.1.5; HLDs) are enzymes belonging to the α/β-hydrolase family, which cleave carbon-halogen bonds in a broad spectrum of chlorinated, brominated and iodinated substrates. HLDs are used in a wide range of applications in biocatalysis, bioremediation, biosensing and cellular imaging [1]. HLDs structurally belong to the α/β-hydrolase superfamily with a three-dimensional structure composed of two domains: (i) the conserved α/β-hydrolase main domain and (ii) the helical cap domain, variable in terms of a number and the arrangement of secondary elements. The active site is deeply buried at the domains interface and is connected with the surrounding environment by access tunnels. HLDs possess a pentad of essential amino acids composed of a catalytic triad and a pair of halide-stabilizing residues. The catalytic triad comprises a nucleophile, a catalytic base, and a catalytic acid. The composition of the catalytic pentad varies among subfamilies: Asp-His-Asp + Trp-Trp in subfamily HLD-I, Asp-His-Glu + AsnTrp/Tyr in subfamily HLD-II, and Asp-His-Asp + Asn-Trp in subfamily HLD-III [4]. The catalytic mechanism of HLDs consists of two chemical steps. In the first step, nucleophilic cleavage of a carbon-halogen bond leads to the formation of an ester intermediate and a halide ion. In the second step, intermediate hydrolysis yields the corresponding alcohol and a proton [2,3]. More than three decades of experimental and *in silico* research on HLDs has made them the benchmark enzymes for

* Corresponding authors at: Loschmidt Laboratories, Department of Experimental Biology and RECETOX, Masaryk University, Kamenice 5/A13, 625 00 Brno, Czech Republic (Z. Prokop) and Department of Chemistry and RECETOX, Masaryk University, Kamenice 5, 625 00 Brno, Czech Republic (P. Klán).
E-mail addresses: klan@sci.muni.cz (P. Klán), zbynek@chemi.muni.cz (Z. Prokop).

https://doi.org/10.1016/j.csbj.2020.03.029
2001-0370/

studying structure–function relationships of >100.000 members of the α/β-hydrolase superfamily [4,5] and the development of a novel *in silico* methods in the fields of protein engineering [6,7] and rational protein design [8,9]. Recently, HLDs have become an interesting model for exploring the role of protein dynamics, hydration [10,11] and molecular gating [12–14] in enzyme catalysis. The mechanistic understanding of enzyme catalysis has improved by experimental techniques such as pre-steady-state kinetics [15–17] and single-molecule analyses [11]. The effectivity of these techniques often relies on the physicochemical nature of specific molecular probes. Particularly, fluorescent substrates are powerful reporter systems that provide a direct readout of enzymatic turnovers without the need for artificial protein labeling [18]. Detectable changes in fluorescence intensity, anisotropy or lifetime can provide useful information about individual processes during a catalytic cycle, e.g., substrate/product transport and binding interactions, individual chemical steps, and the role of solvent and protein dynamics. However, such probes are only available for certain classes of enzymes, e.g., lipases [19–21], esterases [21], alkaline phosphatase [22] and β-galactosidase [23].

In this study, we present the development of the first fluorescent substrates for HLDs which change their spectral properties during the enzymatic reaction, providing a distinctive signal for specific steps of the catalytic cycle. The probes were based on coumarin and BODIPY (4,4-difluoro-4-bora-3a,4a-diaza-*s*-indacene) chromophores. Activity screening with a set of well-characterized HLDs demonstrated their broad applicability within the enzyme family. Detailed kinetic measurements of the reactions of selected enzymes with these newly introduced fluorescent molecules provided an outstanding level of information, particularly when combined with rapid mixing techniques. Moreover, we demonstrated efficient protein labeling by tracking their conversion into the corresponding ester intermediates when incubated with HLDs with mutated catalytic histidine. These molecules specifically attach in the active site and can serve as probes for studying protein hydration and dynamics as well as potential markers for cell imaging.

2. Results and discussion

2.1. Characterization of fluorescent substrates

Inspired by the results of our previous study focused on the application of virtual screening for the identification of novel HLDs substrates [24], we tested four commercially available coumarin-based halogenated molecules (Fig. S1). The 4-(halomethyl) groups of the selected coumarin molecules were intended to be sites of enzymatic dehalogenation. Chemical changes occurring in this group (esterification, hydrolysis) [25] should ideally be reflected by shifts in the emission band maxima (λ_{max}) and/or changes in emission intensities. All four 4-(halomethyl) coumarin derivatives were active with HLDs. Since 4-(bromomethyl)-6,7-dimethoxycou marin (COU–Br) provided a significant spectral change during the enzymatic reaction, it was selected as an enzyme activity probe for detailed characterization (Fig. 1A).

Subsequently, we applied the same strategy using a more stable BODIPY fluorophore. We designed and synthesized [25,26] two 8-chloromethyl-BODIPY derivatives and one 8-iodomethyl-BODIPY derivative (Fig. S2). Our tests of HLD activity toward these probes indicated they were good candidates combining high conversion rates and significant spectral changes during the enzymatic reaction. Finally, BDP–Cl was selected as the best candidate for further detailed characterization (Fig. 1B). This molecule provides a high conversion rate across a broad range of HLDs. Both COU–Br and BDP–Cl substrates significantly increased their fluorescence intensity after cleavage of halide ion to give the corresponding product.

Enzymatic dehalogenation occurs in four essential steps (Scheme 1). After the substrate (fluorescent probe) PX is transported to the enzyme HLD cavity (k_1), a covalently bound ester intermediate HLD–P is formed by nucleophilic attack of the carboxylate oxygen of an aspartate group on the carbon atom of the substrate and subsequent cleavage of the carbon-halogen bond (k_2). The ester intermediate bears the probe, which shows an altered fluorescent signal due to its chemical modification. In the third step, the ester intermediate is hydrolyzed by a water molecule activated by histidine as a catalytic base. During the hydrolytic step, the probe is released as a differently emitting alcohol POH (k_3). The last step recovers HLD when products of the catalytic reaction are liberated from the enzyme cavity (k_4). If the emission of all the probe derivatives is distinguishable, the probe can be used to monitor the individual reaction steps and determine the reaction rate constants.

Based on the catalytic cycle, we prepared fluorescent probes in the form of their reaction intermediates COU–HLD (Fig. 1C) and BDP–HLD (Fig. 1D), model acetate BDP–OAc mimicking the alkyl-enzyme intermediate and the corresponding alcohols COU–OH (Fig. 1E) and BDP–OH (Fig. 1F) to evaluate their fluorescent properties, i.e., emission band maxima (λ^{fl}_{max}) and quantum yields of fluorescence (Φ_{fl}) (Table 1). The alkyl-enzyme intermediates COU–HLD and BDP–HLD were prepared by enzymatic reaction of COU–Br and BDP–Cl substrates with a mutant, lacking the catalytic histidine, so the reaction spontaneously stops after the first chemical step at the form of covalently-bond intermediate. The λ^{fl}_{max} values of coumarin and BODIPY derivatives exhibited only modest variations. However, both COU–Br and BDP–Cl substrates significantly increase their quantum yield (Φ_{fl}) after the cleavage of halogen ion. Additionally, the quantum yield of BDP also significantly differs for enzyme-ester intermediate (BDP-OAc) and product (BDP-OH) which makes this probe highly attractive for sensitive monitoring of individual reaction steps.

The experiments were carried out at pH 8.0 and temperature of 30 °C, which is optimal for the activity of most HLDs. Under these conditions, both dyes showed sufficient chemical stability. The derivatives COU–Br and BDP–Cl were stable in the dark (Fig. S4) and slowly degraded under irradiation from a light source (Fig. S5), which was incomparably stronger than the probe light used for the kinetic experiments. The changes in the fluorescence spectra of BDP–Cl were related to aggregation in aqueous solution (Fig. S4D) kept in the dark. The use of a co-solvent was necessary due to the limited solubility of the fluorescent probes. DMSO was chosen as an organic solvent which is well tolerated by most HLDs [27]. No more than 10 % of DMSO was used in the experiments to minimize the influence of organic solvents on enzyme activity and stability.

2.2. Activity screening

The broad applicability of our fluorescent substrates was tested by screening the activity of a representative set of wild type HLDs: DatA from *Agrobacterium tumefaciens* C58 [28], DbeA from *Bradyrhizobium elkani* USDA94 [29], DbjA from *Bradyrhizobium japonicum* USDA110 [30], DhaA from *Rhodococcus rhodochrous* NCIMB 13064 [31], DhlA from *Xanthobacter autotrophicus* GJ10 [32], DmmA from a marine microbial consortium [33] and LinB from *Sphingobium japonicum* UT26 [34]. The set of HLDs included enzymes of diverse origin, specificity and structural characteristics, such as shape and size of entrance tunnels and active sites [1]. Two enzymes, DmmA and LinB, exhibited specific activity toward both fluorescent substrates COU–Br and BDP–Cl comparable with the activity toward 1-chlorobutane and 1,2-dibromoethane, the best chlorinated and brominated substrates reported so far for this

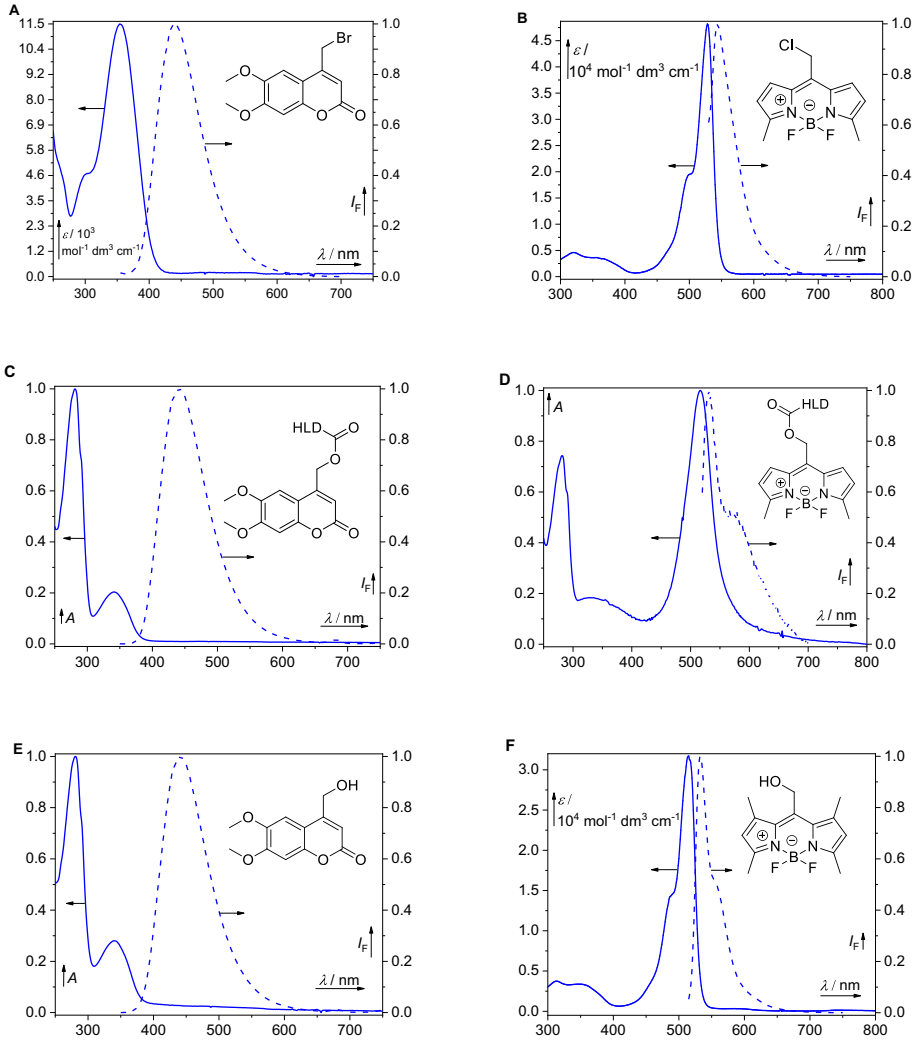

Fig. 1. Absorption and emission spectra of selected fluorescent substrates. Absorption (solid lines, left ordinate) and normalized emission (fluorescence intensity, dashed lines, $\lambda_{exc(A)}$ = 350 nm, $\lambda_{exc(B)}$ = 515 nm, right ordinate) spectra of 10 μM COU–Br (A) and 10 μM BDP–Cl (B). Normalized absorption (solid line, left ordinate) and normalized emission spectra (dashed line, λ_{exc} = 340 nm, right ordinate) of 10 μM COU-DmmA. H275F intermediate (C). Normalized absorption (solid line, left ordinate) and normalized emission (dashed line, λ_{exc} = 515 nm, right ordinate) spectra of 7 μM BDP-DhaA130 intermediate (D). Normalized absorption (solid line, left ordinate) and normalized emission (dashed line, λ_{exc} = 340 nm, right ordinate) spectra of 10 μM coumarin product (E). Absorption (solid line, left ordinate) and normalized emission (dashed line, λexc = 500 nm, right ordinate) spectra of 10 μM BDP product (F). All spectra measured in PBS buffer/DMSO mixture (90:10, v/v), pH 8.0.

enzyme family (Fig. 2, Table S1). Intriguingly, the activities toward COU–Br were the highest reported for both LinB and DmmA enzymes [35,36]. The extraordinary activity of DmmA toward such bulky substrates was previously described by Buryska et al. [35] and is most likely due to the unusually wide active site of this specific dehalogenase. The high activity of LinB with the bulky BDP–Cl and COU–Br is likely linked to the prominent dynamics of this enzyme variant. On the other hand, the lowest activity was identified for reactions with DatA, which corresponds to a rare combination of halide stabilizing residues and a small volume active site cavity [36]. Notably, a weak activity of DhlA toward both fluorescent substrates was also detected, even though this enzyme has the smallest active site within the HLD family and a narrow tunnel evolved for the conversion of the small molecule 1,2-dichloroethane. This result confirms that the specificity-determining cap domain of DhlA can undergo large conformational changes to accommodate bulky substrates [37].

2.3. Steady-state kinetics

The most active enzymes, DmmA and LinB, were selected for steady-state kinetic analysis. Fluorescence conversion curves recorded at different substrate concentrations (Figs. S6-7) were fitted globally using a steady-state kinetic model (Scheme S1). This analysis provided a quick and convenient estimate of the steady-state kinetic parameters (Table 2 and Table S2). The reaction of LinB and DmmA with both fluorescent substrates BDP–Cl and COU–Br showed a micromolar range of Michaelis-Menten constant (K_m), representing the lowest values reported to date for the HLD family (K_m for standard small substrates ranges from 400 to 2 500 μM for DmmA [35] and 5 to 2 000 μM for LinB [1]). These results imply that the bulky fluorescent substrates might be structurally closer to natural substrates of these specific dehalogenases than the relatively small halogenated molecules reported as representative substrates for HLDs. The natural reaction of DmmA is unknown, whereas LinB converts bulkier 1,3,4,6-tetrachloro-1,4-cyclohexadiene and 2,4,5-trichloro-2,5-cyclohexadiene-1-ol within a pathway for the degradation of lindane (1,2,3,4,5,6-hexachlorocyclohexane) [38]. Turnover numbers k_{cat} were comparable with those reported previously for representative substrates [1,6,35]. The high affinity with the retained turnover number provided superior specificity for the conversion of both fluorescent substrates: k_{cat}/K_m ranging from 0.14 to 12.6 μM^{-1} s^{-1}, compared to three orders of magnitude lower specificity for the conversion of

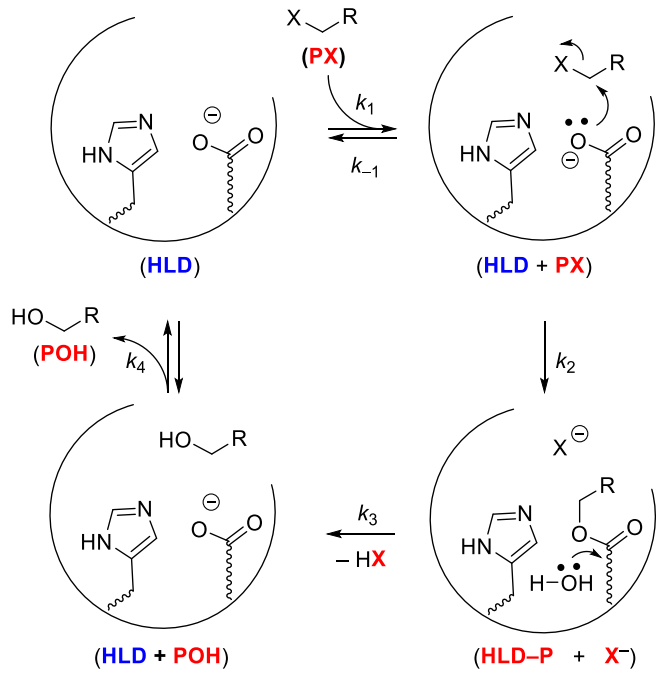

Scheme 1. Schematic of the catalytic cycle of HLDs. The catalytic cycle of HLD in reaction with fluorescent halogenated probe PX (R = COU or BDP; X = Cl, Br or I). HLD-P is an alkyl enzyme intermediate, POH is the alcohol product. The reaction mechanism for HLDs has been proposed based on X-ray crystallographic [2] and pre-steady state kinetic studies [15,16].

Table 1
Photophysical properties of fluorescent substrates.[a]

	λ_{max}/nm[b]	ε/M^{-1}cm^{-1}[c]	λ^{fl}_{max}/nm[b]	Φ_{fl}/%[b]
COU–Br	354	11,500	440	15.2 ± 1.2
COU–HLD	281/342	n.d.	443	83.2 ± 2.5
COU–OH	281/342	n.d.	443	85.3 ± 0.6
BDP–Cl	528	48,177	544	26.1 ± 0.8
BDP–OAc	520	46,437	536	68.0 ± 1.0
BDP–HLD	281/516	n.d.	531	49.4 ± 2.1
BDP–OH	515	31,705	533	92.1 ± 4.3

[a] The absorption (λ_{max}) and emission (λ^{fl}_{max}) maxima, molar absorption coefficients (ε), and quantum yields (Φ_{fl}) were measured for both substrates COU–Br and BDP–Cl and hydrolytic products COU–OH and BDP–OH. The photophysical properties of alkyl-enzyme intermediates COU–HLD and BDP–HLD were tested after enzymatic reaction of COU–Br and BDP–Cl substrates with a catalytic histidine mutant, stopping the reaction at the intermediate form. The acetic acid ester of BDP (BDP–OAc) was synthesized to mimic the alkyl-enzyme intermediate (Fig. S3).
[b] Solutions in a PBS buffer/DMSO mixture (90:10, v/v), pH = 8.0, c ≈ 10^{-6} M.
[c] Determined in neat DMSO from three independent measurements; n.d. – not determined.

representative substrates 1,2-dibromoethane and 1-chlorobutane. Substrate inhibition was observed in the reaction of DmmA with BDP–Cl. The kinetic analysis using the extended kinetic model (Scheme S1B) provided equilibrium constant for dissociation of substrate inhibitory complex K_{SI} = 3.1 ± 0.9 μM.

2.4. Pre-steady-state kinetics

Pre-steady-state kinetic experiments were conducted to gain deeper insights into the kinetic mechanism of DmmA and LinB (Scheme 1) during the conversion of BDP–Cl and COU–Br. Single and multiple turnover conditions were used to obtain information about all kinetically significant catalytic steps, as well as to examine their dependence on substrate concentrations. In the case of BDP–Cl, single and multiple turnover experiments were performed by applying two excitation wavelengths of 500 and 280 nm for specific excitation of the fluorescent substrate and tryptophan residues, respectively. The excitation at 500 nm provided information about chemical changes occurring on the substrate (P–X → HLD–P → P–OH, Table 1), whereas excitation at 280 nm enabled monitoring transport processes, substrate binding and product release by using fluorescence resonance energy transfer (FRET) between intrinsic tryptophan (Trp) of enzyme and fluorescent substrate BDP–Cl. Due to dominant absorption of enzyme Trp at 280 nm (Fig. S8A) and the location of the BDP–Cl excitation band in the region of tryptophan emission (~450 nm), a halide-stabilizing tryptophan residue located in the active site cavity was utilized as a FRET donor to transfer the energy to bound BDP–Cl. Absorption and emission spectra of BDP–Cl and tryptophan and the region of the donor to acceptor energy transfer are illustrated in Supporting Fig. S8B. A similar approach was applied to COU–Br measurements. The excitation at 345 nm provided information about chemical changes occurring on the substrate, however, no significant FRET signal was observed as the excitation spectra of COU–Br and tryptophan with a lower quantum yield largely overlapped.

The reaction of DmmA with BDP–Cl produced a strong signal at both excitation wavelengths (Fig. 3). We assigned the enhancement of fluorescence signal at 500 nm to the transformation of the substrate (P–X) to a covalently bound ester intermediate (HLD–P) and its further enhancement to hydrolysis of this intermediate to the final alcohol product (P–OH). This assignment was based on the distinctive fluorescence quantum yields of the model probe derivatives shown in Table 1. The data measured at 280 nm additionally provided information on the substrate binding and product release (Fig. 3C, D). An initial increase of fluorescence intensity corresponded to binding of BDP–Cl in the active site leading to the approach of BDP–Cl and tryptophan into the efficient FRET distance. The following linear phase in multiple turnover traces represented the consecutive catalytic cycles in which the highly emissive product was formed and the overall fluorescence intensity of the reaction mixture was enhanced. Finally, product release was accompanied by a reduction of FRET efficiency, resulting in a decrease of the fluorescence signal.

In the case of DmmA reaction with COU–Br, the fluorescence signal recorded upon excitation at 345 nm was used to monitor chemical changes occurring on COU (Fig. S9). The lag of the signal change at the beginning of the reaction is related to the substrate binding preceding the chemical conversion, which produces the increase in fluorescence signal. Due to the overlap of excitation spectra of COU–Br and tryptophan, the FRET signal providing additional information about substrate/product transport could not be obtained. In comparison to BDP–Cl, the amount of information from the available fluorescence signal was lower. The similar value of quantum yield for the intermediate and product did not allow distinction between the last kinetic steps (i.e., hydrolysis and product release). The only simplified three-step model was supported by the kinetic data including (i) substrate binding, (ii) cleavage of carbon halogen bond and (iii) the last step leading to a free enzyme which might be determined either by hydrolysis or product release process.

Similar data were obtained for the reaction of LinB with BDP–Cl and COU–Br (Figs. S10–11). For BDP–Cl, the signal measured upon excitation at 280 nm showed clear kinetic phase related to the substrate binding. However, the following part of the time course significantly differed from kinetic traces obtained for reaction with DmmA. The strong rise and decay of the signal recorded with DmmA were not observed for LinB and only slow single exponential increase with low signal amplitude was obtained for reaction of LinB. The time course together with the magnitude of the signal indicates transient accumulation of the highly fluorescent alkyl-

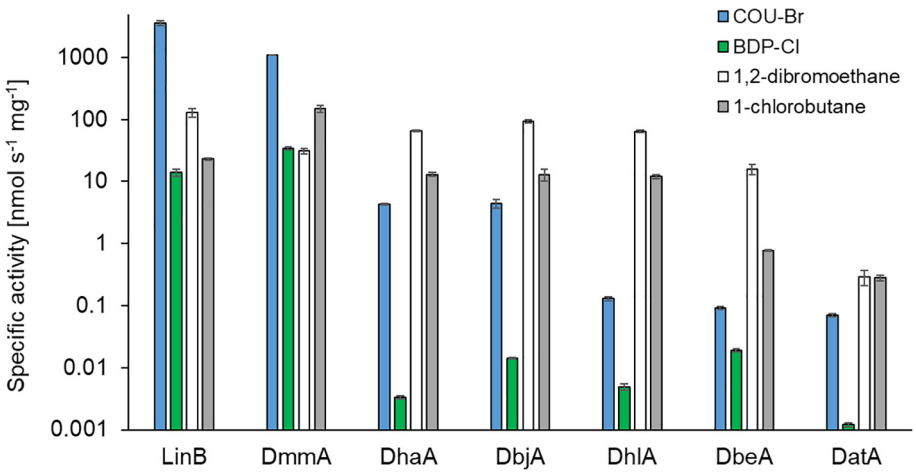

Fig. 2. Specific activities of wild type HLDs. Specific activities with standard errors for selected HLDs with COU–Br (blue) and BDP–Cl (green) recorded by fluorescence measurement compared with activities toward reference substrates 1,2-dibromoethane (white) and 1-chlorobutane (grey) recorded by standard colorimetric assay [28,35,36]. (For interpretation of the references to colour in this figure legend, the reader is referred to the web version of this article.)

Table 2
Steady-state kinetic parameters.[a]

Substrate	Enzyme	K_m/μM	k_{cat}/s^{-1}	K_P/μM	k_{cat}/K_m/μM^{-1} s^{-1}
BDP–Cl	DmmA[b]	0.23 ± 0.07	2.9 ± 0.6	0.09 ± 0.03	12.6
	LinB	17 ± 1	2.3 ± 0.2	11 ± 1	0.14
COU–Br	DmmA	0.9 ± 0.6	1.9 ± 0.1	1.4 ± 0.9	2.1
	LinB	0.7 ± 0.5	3.9 ± 0.2	0.5 ± 0.3	5.6
DBE	LinB [6]	1700 ± 200	12 ± 4	n.a.	0.007
	DmmA [35]	2300 ± 300	1.8 ± 0.4	n.a.	0.0008
CB	LinB [39]	240 ± 20	1.00 ± 0.03	n.a.	0.004
	DmmA [35]	400 ± 100	0.17 ± 0.02	n.a.	0.0004

[a] Michaelis-Menten constant (K_m), turnover number (k_{cat}), and specificity constant (k_{cat}/K_m) and equilibrium dissociation constant for enzyme-product complex (K_P) for the reaction of LinB and DmmA with BDP–Cl and COU–Br at 30 °C, and pH 8.0 and 1,2-dibromoethane (DBE) and 1-chlorobutane (CB) at 37 °C and pH 8.6.
[b] Substrate inhibition observed with dissociation of inhibitory complex K_{SI} = 3.1 ± 0.9 μM. n.a. not available, the steady-state kinetics analyzed by initial rate estimation did not provide product inhibition information. The fitted parameters with complete statistics are summarized in Supporting Table S2.

enzyme intermediate during the conversion of BDP–Cl by DmmA. The accumulation of enzyme-intermediate implies that the initial steps, the substrate binding and the cleavage of the carbon-halogen bond, are faster than the following hydrolysis or product release. The reaction with LinB does not show such an accumulation of the intermediate, suggesting that the carbon-halogen bond cleavage is the slow rate-limiting step followed by faster hydrolysis and product release. This observation was supported by the data recorded upon excitation at 500 nm when both alkyl-enzyme intermediate and product formation can be monitored. DmmA showed fast and slow phase related to the fast formation of the intermediate while only a single slow phase was observed for LinB.

The data recorded for the reaction of LinB with COU–Br are similar to those obtained for DmmA. The fluorescence signal recorded upon excitation at 345 nm showed a lag related to substrate binding preceding chemical slow exponential increase of fluorescence signal related to the chemical conversion of COU–Br to intermediate and product.

The results of the global fit analysis provided the rate constants for individual reaction steps (Table 3) of the catalytic cycle shown in Scheme 1. A minimal four-step model (Scheme S2) provided good simultaneous fit of all kinetic data, steady- and pre-steady-state, obtained for reaction of LinB with BDP–Cl. The extended model (Scheme S3) including additional inhibitory effects of the product was used to fit steady-state as well as pre- steady-state data obtained for reaction of DmmA and BDP–Cl (Scheme S3). The kinetic data obtained in the reaction of DmmA and LinB with COU–Br supported only a simplified three-step catalytic cycle, which was also extended by the inhibitory effect of an alcohol product.

Two different rate-limitations were observed in the analysed reactions. Nucleophilic cleavage of the carbon-bromine bond was the slowest process in the conversion of COU–Br by both tested enzymes and in the reaction of LinB with BDP–Cl. In the case of DmmA reaction with BDP–Cl, the catalytic cycle was limited by slow product release. Slow kinetic phases were also distinguished for substrate binding, suggesting that the transport processes are slow for the bulky BDP–Cl and COU–Br. The slow kinetics were previously described for binding of 1,2-dichloroethane to DhlA with the substantially occluded active site [16]. On the contrary, the rapid equilibrium was described for the binding of the small halogenated substrate by LinB [15]. Interestingly, the observed rate of nucleophilic substitution during BDP–Cl conversion was almost two orders of magnitude faster for DmmA than LinB. This may be related to anatomy and volume of the DmmA active site, which allows for proper reactive orientation of bound BDP–Cl.

Moreover, the substrates showed high affinity towards enzymes with an expected equilibrium dissociation constant for enzyme-substrate complex lower than 1 μM. This strong affinity was indicated for COU–Br towards both tested enzymes LinB and DmmA and BDP–Cl towards DmmA. A weaker affinity was found only for BDP–Cl towards LinB with an equilibrium dissociation constant 38 μM. In accord, the steady-state specificity constants for BDP–Cl

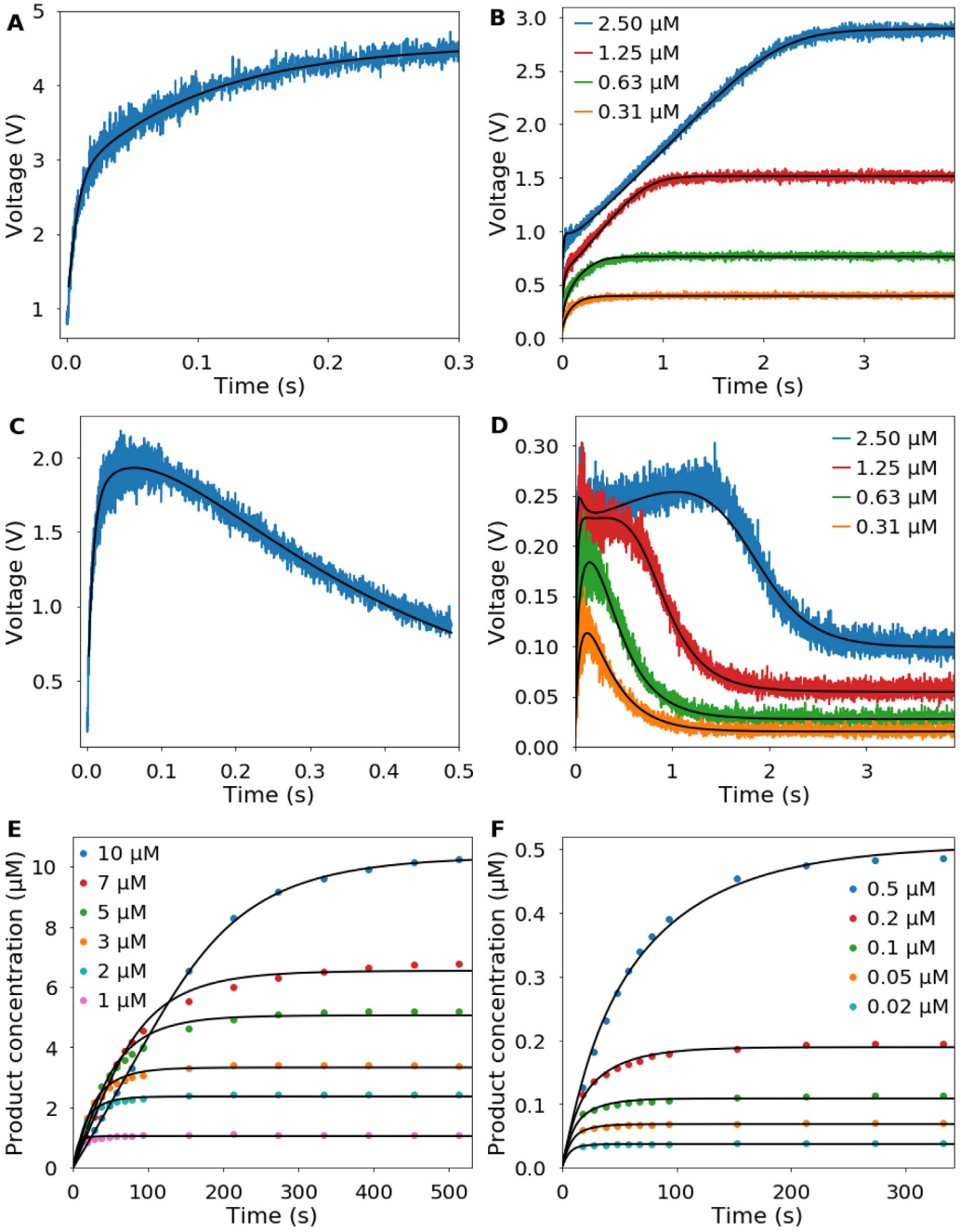

Fig. 3. Pre-steady-state kinetic data of DmmA reaction with BDP–Cl. Stopped-flow fluorescence single turnover experiments were carried out with an excitation wavelength of 500 nm (A) and 280 nm (C) in a combination with 530 nm long-pass filter detection of emitted light for monitoring of BODIPY fluorescence intensity and tryptophan-BODIPY FRET, respectively. The concentration of DmmA and BDP–Cl was 10 μM and 5 μM, respectively. The concentration dependence was analyzed by mixing enzyme at 0.625 μM concentration with different concentrations of BDP–Cl. The concentration dependence data were also recorded for both excitation wavelength of 500 nm (B) and 280 nm (D) with 530 nm long-pass filter for detection of BODIPY fluorescence intensity and FRET, respectively. Each fluorescence trace represents an average of 5–8 replicates. Pre-steady-state kinetic data were fitted simultaneously with steady-state progress curves obtained upon mixing 0.07 μM DmmA with 1 to 10 μM BDP–Cl (E), 0.006 μM DmmA with 0.02 to 0.5 μM BDP–Cl (F) measured at excitation/emission wavelengths 510/530 nm by using microtiter plate spectrofluorometer. The black lines represent the best global fit.

(setting a lower limit for binding step k_1) differ by two orders of magnitude with k_{cat}/K_m value 12.6 $\mu M^{-1}.s^{-1}$ for DmmA and 0.14 $\mu M^{-1}.s^{-1}$ for LinB. The strong binding affinity for the substrate was accompanied by strong product inhibition. The alcohol products, which are hydroxyl derivatives of these complex molecules, kept strong binding interactions similar to the starting halogenated structures. After being released, the alcohol product can re-bind to the enzyme active site providing strong inhibitory complex competing to the formation of the enzyme-substrate complex (Scheme S3 and Tables S3-4). No sign of the additional product inhibitory effect was observed for the reaction of LinB with BDP–Cl, which is in accordance with weak substrate binding. Addition-

Table 3
Kinetic parameters for individual steps of HLDs reaction pathway.[a]

Substrate	Enzyme	$k_1/\mu M^{-1}s^{-1}$	k_{-1}/s^{-1}	k_2/s^{-1}	k_3/s^{-1}	k_4/s^{-1}
BDP–Cl	DmmA	61 ± 1	–[b]	190 ± 10	10.0 ± 0.3	3.34 ± 0.04
	LinB	2.4 ± 0.1	90 ± 3	5.9 ± 0.2	>10	>10
COU–Br	DmmA	2.33 ± 0.02	–[b]	2.40 ± 0.01	5.4 ± 0.1	–[c]
	LinB	6.23 ± 0.05	–[b]	10.0 ± 0.1	21.5 ± 0.2	–[c]
DCE	DhlA	$9 \pm 1 \times 10^{-3}$	20 ± 5	50 ± 10	14 ± 3	8 ± 2
DBP	DhaA	0.8–2.5	60–300	249–272	13.5–16.3	3.4–4.6
CH	LinB	$K_s = k_{-1}/k_1 = 240 \pm 40$ mM[d]		117 ± 5	3.2 ± 0.2	–[c]

[a] Individual rate constants (±standard errors) obtained from a global fit of the kinetic data to the model of the catalytic cycle described in Scheme 1. The kinetic data for BDP–Cl and COU–Br were measured at 30 °C in phosphate buffer (pH 8.0). The reaction of DhlA with 1,2-dichloroethane (DCE) was determined at pH 8.2 and 30 °C [16], the reaction of DhaA with 1,3-dibromopropane (DBP) was determined at pH 9.4 and 30 °C [17], and the reaction of LinB with 1-chlorohexane (CH) was determined at pH 8.6 and 37 °C [15].
[b] The reverse rate was not obtained by the global fit ($k_{-1} \ll k_2$).
[c] A simplified three-step model was applied (step k_4 was not included).
[d] Only a rapid equilibrium for substrate binding was observed, providing the equilibrium constant for dissociation of the enzyme-substrate complex ($K_s = k_{-1}/k_1$). The model included substrate inhibition providing equilibrium dissociation constant $K_{SI} = 2.34 \pm 0.03$ μM. The fitted parameters, scaling factors with complete statistics are summarized in Supporting Tables S3 and S4.

ally, the kinetics of DmmA reaction with BDP–Cl showed substrate inhibition. The substrate might negatively interact with different enzyme forms. The systematic global fitting of steady-state and pre-steady-state data by all possible schemes for substrate binding to ES (enzyme-substrate complex), EI (alkyl-enzyme intermediate) and EP (enzyme-product complex) indicated the EP complex is the most likely inhibited by an excess of the substrate (Supporting Information).

2.5. Protein labeling

Apart from the wide range of applications of HLDs utilizing their ability to convert haloalkanes to alcohols (Scheme 1), they can also serve (after appropriate modification) as protein tags with various linked functionalities, including fluorescence. The HaloTag technology [40] is based on irreversible covalent binding of synthetic ligands to haloalkane dehalogenase DhaA with mutations, includ-

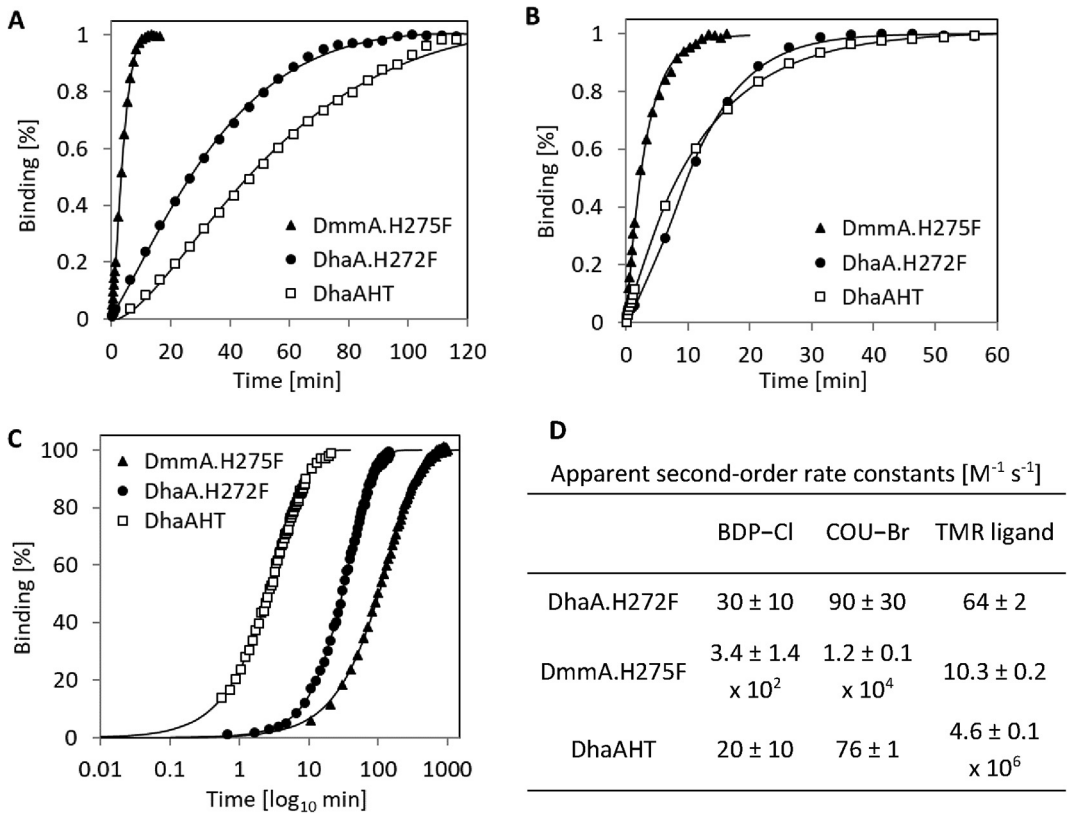

Fig. 4. Binding kinetics of fluorescent probes to selected HLDs. Kinetic data obtained upon mixing 10 μM BDP–Cl with 17.1 μM DmmA.H275F, 16.2 μM DhaA.H272F or 17.9 μM DhaAHT (A). Kinetic data obtained upon mixing 0.25 μM COU–Br with 0.45 μM DmmA.H275F and 10 μM COU–Br with 16.2 μM DhaA.H272F or 17.9 μM DhaAHT (B). Kinetic data obtained upon mixing 5 μM TMR ligand with 11 μM DmmA.H275F or 8.6 μM DhaA.H272F, and 0.5 nM TMR ligand with 1 nM DhaAHT (C). The fluorescence anisotropy was used to monitor TMR ligand binding and the fluorescence intensity to monitor binding of BDP–Cl and COU–Br. All experiments were performed at 30 °C, pH 8.0. Solid lines represent the best fit to the data. Apparent second-order rate constants for the binding of fluorescence probes to the tested enzyme variants containing a mutation in the catalytic histidine (D).

ing the substitution of its conserved catalytic base – H272F. Following this mutation, base-catalyzed hydrolysis (second chemical step) is blocked and the reaction mechanism stops after the alkyl-enzyme intermediate (HLD-P) is formed. To prove the potential applicability of BDP–Cl and COU–Br in protein labeling, a binding kinetic analysis with HLD DmmA.H275F, DhaA.H272F and DhaAHT (H272F + K175M + C176G + Y273L) with mutated catalytic histidine was conducted by tracking the increase in fluorescence intensity upon conversion into the ester intermediate with time (Fig. 4A, and B). The same enzymes were used for reaction with a commercial fluorescent HaloTag tetramethylrhodamine (TMR) ligand. In the case of the TMR ligand, interactions with the enzyme molecules were monitored by changes in fluorescence anisotropy (Fig. 4C) since the formation of the TMR intermediate does not provide any change in fluorescence intensity.

Positive binding was observed with both novel fluorescent substrates BDP–Cl and COU–Br. In both cases, DmmA.H275F with its exceptionally large active site was the most efficient of the tested HLDs, followed by DhaA.H272F and DhaAHT. These results correlate well with the activity screening of wild type HLDs. The most promising was the interaction of DmmA.H275F with COU–Br. The results of TMR ligand binding kinetics showed fast interaction with DhaAHT. This was expected since this protein–ligand variant was engineered based on modeling, site-saturation mutagenesis and high-throughput screening to develop an efficient HaloTag system. For DhaA.H272F and DmmA.H275F, neither of which contains any additional mutations, the binding were slower. Although binding of the fluorescent substrates was not as fast as in the engineered HaloTag technology with TMR ligand, they offer the advantage of easy tracking of fluorescence intensity instead of less sensitive and instrumentally more complex anisotropy/polarization measurements. These probes could present an alternative to HaloTag ligands for cell labeling experiments. However, 6-fold and 2-fold increase in quantum yield upon covalent binding to HLDs in the case of COU–Br and BDP–Cl, respectively, cannot guarantee a no-wash protocol. In comparison, ~20-fold fluorescence intensity increase upon binding of photoactivable Janelia Fluor ligands do not require washing steps which are required for application of TMR ligands [41]. The clear novelty of fluorescent substrates BDP–Cl and COU–Br, without the long reactive linker characteristic of the TMR HaloTag ligand, is that they bind deeper inside the active site cavity (Fig. S12) and can be used as effective probes for monitoring dynamics and hydration [10,11] directly in the catalytically important protein region.

3. Conclusions

The first fluorescent substrates for the HLD enzyme family were developed. Two different probes based on coumarin and BODIPY core structures were characterized and compared. The broad applicability of these fluorescent substrates was tested by screening their activity with a set of seven representative enzymes: DatA, DbeA, DbjA, DhaA, DhlA, DmmA and LinB. Overall, the activity toward both fluorescent substrates was comparable to those obtained with typical substrates (halogenated alkanes) of this enzyme family. The outstanding potential for probing enzyme catalysis using these novel fluorescent substrates was demonstrated by performing a detailed kinetic analysis of the two most active enzymes – LinB and DmmA. Interestingly, the steady-state kinetic analysis showed that both fluorescent substrates provide almost three orders of magnitude higher specificity in comparison to that of the representative halogenated substrates, primarily due to their strong binding affinities in a micromolar range. Importantly, a single stopped-flow experiment can provide direct observation of all involved catalytic steps, substrate binding and product release, as well as chemical processes, by analyzing changes in fluorescence intensities in combination with monitoring FRET efficiencies between the fluorescent reporting molecule and intrinsic Trp residue in the active site.

The fluorescent substrates of HLDs may have wide applicability in various fields. The probes are suitable for screening of HLDs activity ready for high throughput applications in combination with robotic or microfluidic systems. In combination with pre-steady-state kinetic measurements, they provide valuable information on the mechanism of enzyme catalysis, including the effects of transport processes. Additionally, both fluorescent probes exhibit high specificity for active site labeling. Biophysical measurements employing these fluorescent substrates will improve the fundamental understanding of enzyme function and promote the development of novel concepts in the rational design of efficient biocatalysts. We expect that these probes will find broad application in mechanistic studies of the model family and help to elucidate fundamental questions about the role of transport processes, protein dynamics and hydration in enzyme catalysis.

4. Methods

4.1. Synthesis of BDP–Cl (8-chloromethyl-4,4′-difluoro-3,5,-dimethyl-4-bora-3a,4a-diaza-s-indacene)

A solution of chloroacetyl chloride (0.250 mL, 3.14 mmol, 1 equiv.) in dry dichloromethane (1 mL) was added dropwise to a solution of 2-methylpyrrole [42] (0.550 mL, 6.28 mmol, 2 equiv.) in dry dichloromethane (15 mL) under a nitrogen atmosphere at 0 °C for 30 min. The reaction mixture was stirred at room temperature for 12 h. Then, triethylamine (1.1 mL, 7.85 mmol, 2.5 equiv.) and $BF_3{\cdot}Et_2O$ in diethyl ether (46%, 2 mL, 15.7 mmol, 5 equiv.) were added at 0 °C and the resulting mixture was stirred at room temperature for 3 h. Aq. HCl (10%, 10 mL) was added and the crude mixture was extracted with dichloromethane (3 × 10 mL). The collected organic layers were dried over anhydrous magnesium sulfate, filtered and concentrated to dryness under reduced pressure. The product was purified by flash chromatography on silica gel (hexane/dichloromethane, 6:4). Yield 200 mg (24%). Red solid. ^{1}H NMR (300 MHz, $CDCl_3$): δ (ppm) 7.17 (d, J = 4.2 Hz, 2H), 6.33 (d, J = 4.2 Hz, 2H), 4.62 (s, 2H), 2.63 (s, 6H) (Fig. S13). ^{13}C NMR (75 MHZ, $CDCl_3$): δ (ppm) 159.2, 135.7, 134.1, 127.1, 120.0, 37.5, 15.1 (Fig. S14). The spectroscopic data were in good agreement with those reported in the literature [43].

4.2. Enzyme expression and purification

Seven wild-type dehalogenases, i.e., DatA, DbeA, DbjA, DhaA, DhlA, Dmma, LinB, and three HLD variants with mutated histidine, i.e., DhaA.H272F, DhaAHT (H272F + K175M + C176G + Y273L), DmmA.H275F, were expressed in *E.coli* BL21 DE3 cells (DhaA.H272F – BL21 cells) as described previously [28–32,35,44]. The enzymes were purified by metallo-affinity chromatography using a charged Ni-NTA column. Unbound and weakly bound proteins were washed out using purification buffer containing 10 mM imidazole. The target histidine-tagged protein was eluted by increasing the imidazole concentration up to 300 mM and dialyzed overnight against 50 mM phosphate buffer, pH 7.5 (pH 8.0 for protein labeling experiments, 0.01% CHAPS for measurements with TMR ligand). The histidine-tag was not removed. The purity of the prepared proteins was checked by SDS-PAGE.

4.3. Preparation of reaction mixtures

Fluorescent substrate coumarin (Sigma-Aldrich, USA) was dissolved in DMSO and diluted to the required concentration before measurement. For each experiment, a new aliquot of the substrate was prepared. BODIPY substrate was dissolved and stored in MeOH. Before each experiment, the MeOH solution was diluted in DMSO to a final concentration of MeOH less than 1%. The reaction mixture for all experiments consisted of 90 % of 50 mM phosphate buffer, pH 8.0 with enzyme and 10 % of substrate solution in DMSO. For measurements involving the TMR ligand, both the enzyme and substrate solution were diluted in 50 mM phosphate buffer, pH 8.0 with 0.01% CHAPS detergent to minimize non-specific interactions.

4.4. Specific activity assay and steady-state kinetics

Activity measurements and steady-state kinetic experiments were performed in microtiter plates at 30 °C using a Synergy H4 spectrofluorometer (Biotek, USA) equipped with a xenon flash lamp. The reaction was initiated by addition of 20 μl of substrate solution using an automatic dispenser to a total volume of the reaction mixture of 200 μl. Fluorescence intensity was measured from the top using excitation/emission monochromators set to wavelengths 345/437 nm for COU–Br and 510/530 nm for BDP–Cl with a bandwidth of 9 nm. Before measurement, the microtiter plate was shaken for 2 s and then the increase in fluorescence intensity was monitored at regular time intervals. The reaction took place in 8 wells alongside another 8 wells of control measurements (phosphate buffer without enzyme) for monitoring spontaneous hydrolysis of the substrate. Each experiment was independently repeated with 3 different substrate aliquots.

4.5. Pre-steady-state kinetics

Pre-steady-state kinetic experiments were performed using SFM-300 stopped-flow instrument combined with a MOS-500 spectrometer system (BioLogic, France) at 30 °C. Before each experiment, enzyme and buffer solutions were mixed with DMSO and the substrate solution was mixed with phosphate buffer to keep the same composition of solvent in the reaction mixture (10% DMSO and 90% phosphate buffer). All solutions were degassed before the measurement. The reaction was initiated by rapid mixing of the substrate and enzyme in a ratio of 1:1 to a total volume of 150 μl with a total flow rate of 16 mL/s. The mixture in the reaction cuvette was continuously excited by a Xe (Hg) lamp using a wavelength with 2 nm bandwidth selected by a monochromator (345 nm for coumarin, 500 nm for BODIPY or 280 nm for tryptophan excitation). A long-pass filter (435 nm for coumarin, 530 nm for BODIPY) was employed for detection of emitted light. The reaction was monitored by measuring the change of voltage on the photomultiplier tube corresponding to the change of fluorescence intensity accompanying the reaction. The measurement started immediately after mixing with a dead time of 1 ms. Final kinetic traces were calculated as an average of six to ten consecutive mixing runs.

4.6. Data analysis and statistics

The kinetic data were fit globally with the KinTek Explorer program (KinTek, USA), dynamic kinetic simulation program that allowed multiple data sets to be fit simultaneously to a single model. The model was input through simple text description and the program derived the differential equations needed for numerical integration automatically. A reaction mechanism for haloalkane dehalogenase used in this study has been proposed previously based on X-ray crystallographic [2] and pre-steady state kinetic studies with the haloalkane dehalogenases [15,16]. Data fitting used numerical integration of rate equations from an input model searching a set of parameters using the Bulirsch–Stoer algorithm with adaptive step size that produces a minimum χ^2 value calculated by using nonlinear regression based on the Levenberg-Marquardt method [45]. Residuals were normalized by sigma value for each data point. To account for slight variations in the data, enzyme or substrate concentrations were allowed to vary within an interval of ±10% to make the best fits possible. The standard error (S.E.) was calculated from the covariance matrix during nonlinear regression. In addition to S.E. values, more rigorous analysis of the variation of the kinetic parameters was accomplished by confidence contour analysis by using FitSpace Explorer (KinTek, USA) [46]. In this analysis, the lower and upper limits for each parameter were derived from the confidence contours for χ^2 threshold at boundary 0.98 (Supporting Information Tables S2, S3 and S4).

4.7. Protein labeling

Fluorescence anisotropy measurements were carried out in microtiter plates at 30 °C using an Infinite F500 plate reader (Tecan, Männedorf, Switzerland) equipped with appropriate excitation and emission polarizers. The reaction was initiated by adding 100 μl of the TMR ligand to a total volume of the reaction mixture of 200 μl. The binding was monitored by measuring the time course of changes in fluorescence anisotropy at 580 nm measured from the top following excitation at 544 nm. Before the first measurement, the microtiter plate was shaken for 2 s and then the increase in fluorescence polarization was monitored at regular time intervals. The reactions took place in 4 wells alongside 4 wells of abiotic control for background subtraction.

Fluorescence intensity measurements were carried out in microtiter plates at 30 °C using a Synergy H4 spectrofluorometer (Biotek, USA) equipped with a xenon flash lamp. The reaction was initiated by adding 20 μl of a fluorescent substrate to a total volume of 200 μl. The progress of labeling was monitored by changes in the fluorescence intensity measured from the top using excitation/emission monochromators set to wavelengths 345/437 for COU–Br and 510/530 nm for BDP–Cl with a bandwidth of 9 nm. Before the first measurement, the microtiter plate was shaken for 2 s and then the increase in fluorescence intensity was monitored at regular time intervals. The reaction took place in 4 wells alongside 4 wells of control for monitoring spontaneous hydrolysis of the probes.

Author contribution

JD, PK, and ZP conceived and designed the study. TB performed the initial screening of coumarin dyes and ZD developed and optimized activity and kinetics assays. VD performed the activity screening, steady-state and pre-steady-state kinetics experiment, VD and ZP performed the global analysis of kinetic data. MS performed the protein labelling experiments, ZP analysed obtained binding data. EMS and EP performed the chemical synthesis, EMS characterized all dyes. PK, VD and ZP wrote the manuscript. All authors reviewed the results and contributed to the finalization of the manuscript.

Acknowledgements

The authors would like to express their thanks to the Czech Ministry of Education, Youth and Sports (the RECETOX research infrastructure LM2018121 and the CETOCOEN EXCELLENCE Teaming 2 project 02.1.01/0.0/0.0/18_046/ 0015975) and the European Commission Horizon 2020 Programme (grants 720776 and 814418). Support for this work was also provided by the Czech Science Foundation (GA18-12477S; PK). The authors would like to express their gratitude to all four anonymous referees for many constructive suggestions. We found the comments extremely constructive and helpful. Their implementation improved the manuscript tremendously.

Appendix A. Supplementary data

Supplementary data to this article can be found online at https://doi.org/10.1016/j.csbj.2020.03.029.

References

[1] Koudelakova T, Bidmanova S, Dvorak P, Pavelka A, Chaloupkova R, Prokop Z, et al. Haloalkane dehalogenases: biotechnological applications. Biotechnol J 2013;8:32–45.
[2] Verschueren KHG, Seljée F, Rozeboom HJ, Kalk KH, Dijkstra BW. Crystallographic analysis of the catalytic mechanism of haloalkane dehalogenase. Nature 1993;363:693–8.
[3] Damborský J, Koca J. Analysis of the reaction mechanism and substrate specificity of haloalkane dehalogenases by sequential and structural comparisons. Protein Eng 1999;12:989–98.
[4] Kokkonen P, Koudelakova T, Chaloupkova R, Daniel L, Prokop Z, Damborsky J. Structure-function relationships and engineering of haloalkane dehalogenases. In: Rojo F, editor. Aerobic utilization of hydrocarbons, oils and lipids. Cham: Springer International Publishing; 2017. p. 1–21.
[5] Jindal G, Slanska K, Kolev V, Damborsky J, Prokop Z, Warshel A. Exploring the challenges of computational enzyme design by rebuilding the active site of a dehalogenase. Proc1 Natl Acad Sci 2019;116:389–94.
[6] Brezovsky J, Babkova P, Degtjarik O, Fortova A, Gora A, Iermak I, et al. Engineering a de Novo Transport Tunnel. ACS Catal 2016;6:7597–610.
[7] Pavlova M, Klvana M, Prokop Z, Chaloupkova R, Banas P, Otyepka M, et al. Redesigning dehalogenase access tunnels as a strategy for degrading an anthropogenic substrate. Nat Chem Biol 2009;5:727–33.
[8] Chovancova E, Pavelka A, Benes P, Strnad O, Brezovsky J, Kozlikova B, Gora A, Sustr V, Klvana M, Medek P, Biedermannova L, Sochor J & Damborsky J (2012) CAVER 3.0: a tool for the analysis of transport pathways in dynamic protein structures. PLoS Comput Biol 8, e1002708.
[9] Bednar D, Beerens K, Sebestova E, Bendl J, Khare S, Chaloupkova R, et al. FireProt: energy- and evolution-based computational design of thermostable multiple-point mutants. PLoS ComputBiol 2015;11:e1004556.
[10] Amaro M, Brezovský J, Kováčová S, Sýkora J, Bednář D, Němec V, et al. Site-specific analysis of protein hydration based on unnatural amino acid fluorescence. J Am Chem Soc 2015;137:4988–92.
[11] Sykora J, Brezovsky J, Koudelakova T, Lahoda M, Fortova A, Chernovets T, et al. Dynamics and hydration explain failed functional transformation in dehalogenase design. Nat Chem Biol 2014;10:428.
[12] Kokkonen P, Sykora J, Prokop Z, Ghose A, Bednar D, Amaro M, et al. Molecular gating of an engineered enzyme captured in real time. J Am Chem Soc 2018;140:17999–8008.
[13] Prokop Z, Gora A, Brezovsky J, Chaloupkova R, Stepankova V, Damborsky J. Engineering of protein tunnels: keyhole-lock-key model for catalysis by the enzymes with buried active sites. In: Protein engineering. Handbook Wiley-VCH; 2012. p. 421–64.
[14] Gora A, Brezovsky J, Damborsky J. Gates of Enzymes. Chem. Rev. 2013;113:5871–923.
[15] Prokop Z, Monincová M, Chaloupková R, Klvaňa M, Nagata Y, Janssen DB, et al. Catalytic mechanism of the haloalkane dehalogenase LinB from *Sphingomonas paucimobilis* UT26. J Biol Chem 2003;278:45094–100.
[16] Schanstra JP, Kingma J, Janssen DB. Specificity and kinetics of haloalkane dehalogenase. J Biol Chem 1996;271:14747–53.
[17] Bosma T, Pikkemaat MG, Kingma J, Dijk J, Janssen DB. Steady-state and pre-steady-state kinetic analysis of halopropane conversion by a *Rhodococcus* Haloalkane Dehalogenase†. Biochemistry 2003;42:8047–53.
[18] Turunen P, Rowan AE, Blank K. Single-enzyme kinetics with fluorogenic substrates: lessons learnt and future directions. FEBS Lett 2014;588:3553–63.
[19] Duque M, Graupner M, Stütz H, Wicher I, Zechner R, Paltauf F, et al. New fluorogenic triacylglycerol analogs as substrates for the determination and chiral discrimination of lipase activities. J Lipid Res 1996;37:868–76.
[20] Basu D, Manjur J, Jin W. Determination of lipoprotein lipase activity using a novel fluorescent lipase assay. J Lipid Res 2011;52:826–32.
[21] Sicart R, Collin M-P, Reymond J-L. Fluorogenic substrates for lipases, esterases, and acylases using a TIM-mechanism for signal release. Biotechnol J 2007;2:221–31.
[22] Hill HD, Summer GK, Waters MD. An automated fluorometric assay for alkaline phosphatase using 3-O-methylfluorescein phosphate. Anal Biochem 1968;24:9–17.
[23] Urano Y, Kamiya M, Kanda K, Ueno T, Hirose K, Nagano T. Evolution of fluorescein as a platform for finely tunable fluorescence probes. J Am Chem Soc 2005;127:4888–94.
[24] Daniel L, Buryska T, Prokop Z, Damborsky J, Brezovsky J. Mechanism-based discovery of novel substrates of haloalkane dehalogenases using *in silico* screening. J Chem Inf Model 2015;55:54–62.
[25] Slanina T, Shrestha P, Palao E, Kand D, Peterson JA, Dutton AS, et al. In search of the perfect photocage: structure-reactivity relationships in *meso*-methyl BODIPY photoremovable protecting groups. J Am Chem Soc 2017;139:15168–75.
[26] Al Anshori J, Slanina T, Palao E, Klán P. The internal heavy-atom effect on 3-phenylselanyl and 3-phenyltellanyl BODIPY derivatives studied by transient absorption spectroscopy. Photochem. Photobiol. Sci. 2016;15:250–9.
[27] Stepankova V, Damborsky J, Chaloupkova R. Organic co-solvents affect activity, stability and enantioselectivity of haloalkane dehalogenases. Biotechnol J 2013;8:719–29.
[28] Hasan K, Fortova A, Koudelakova T, Chaloupkova R, Ishitsuka M, Nagata Y, et al. Biochemical characteristics of the novel haloalkane dehalogenase DatA, isolated from the plant pathogen *Agrobacterium tumefaciens* C58. Appl Environ Microbiol 2011;77:1881–4.
[29] Prudnikova T, Mozga T, Rezacova P, Chaloupkova R, Sato Y, Nagata Y, et al. Crystallization and preliminary X-ray analysis of a novel haloalkane dehalogenase DbeA from *Bradyrhizobium elkani* USDA94. Acta Crystallogr, Sect F Struct Biol Cryst Commun 2009;65:353–6.
[30] Sato Y, Monincova M, Chaloupkova R, Prokop Z, Ohtsubo Y, Minamisawa K, et al. Two rhizobial strains, Mesorhizobium loti MAFF303099 and Bradyrhizobium japonicum USDA110, encode haloalkane dehalogenases with novel structures and substrate specificities. Appl Environ Microbiol 2005;71:4372–9.
[31] Kulakova AN, Larkin MJ, Kulakov LA. The plasmid-located haloalkane dehalogenase gene from Rhodococcus Rhodochrous NCIMB 13064. Microbiology 1997;143:109–15.
[32] Keuning S, Janssen DB, Witholt B. Purification and characterization of hydrolytic haloalkane dehalogenase from Xanthobacter autotrophicus GJ10. J Bacteriol 1985;163:635–9.
[33] Gehret JJ, Gu L, Geders TW, Brown WC, Gerwick L, Gerwick WH, et al. Structure and activity of DmmA, a marine haloalkane dehalogenase: DmmA. A marine haloalkane dehalogenase. Protein Sci 2012;21:239–48.
[34] Nagata Y, Miyauchi K, Damborsky J, Manova K, Ansorgova A, Takagi M. Purification and characterization of a haloalkane dehalogenase of a new substrate class from a gamma-hexachlorocyclohexane-degrading bacterium, Sphingomonas paucimobilis UT26. Appl Environ Microbiol 1997;63:3707–10.
[35] Buryska T, Babkova P, Vavra O, Damborsky J, Prokop Z. A haloalkane dehalogenase from a marine microbial consortium possessing exceptionally broad substrate specificity. Appl Environ Microbiol 2017;84:e01684–e1717.
[36] Koudelakova T, Chovancova E, Brezovsky J, Monincova M, Fortova A, Jarkovsky J, et al. Substrate specificity of haloalkane dehalogenases. Biochem. J. 2011;435:345–54.
[37] Kokkonen P, Bednar D, Dockalova V, Prokop Z, Damborsky J. Conformational changes allow catalysis of bulky substrates by a haloalkane dehalogenase with a small and buried active site. J Biol Chem 2018;29:11505–12.
[38] Nagata Y, Endo R, Ito M, Ohtsubo Y, Tsuda M. Aerobic degradation of lindane (γ-hexachlorocyclohexane) in bacteria and its biochemical and molecular basis. Appl Microbiol Biotechnol 2007;76:741–52.
[39] Chaloupková R, Sýkorová J, Prokop Z, Jesenská A, Monincová M, Pavlová M, et al. Modification of activity and specificity of haloalkane dehalogenase from *Sphingomonas paucimobilis* UT26 by engineering of its entrance tunnel. J Biol Chem 2003;278:52622–8.
[40] Los GV, Encell LP, McDougall MG, Hartzell DD, Karassina N, Zimprich C, et al. HaloTag: a novel protein labeling technology for cell imaging and protein analysis. ACS Chem Biol 2008;3:373–82.
[41] Grimm JB, English BP, Chen J, Slaughter JP, Zhang Z, Revyakin A, et al. General method to improve fluorophores for live-cell and single-molecule microscopy. Nat. Methods 2015;12:244–50.
[42] Shin J-Y, Patrick BO, Dolphin D. Self-assembly via intermolecular hydrogen-bonding between o-/m-/p-NH2 and BF2 groups on dipyrromethenes. Tetrahedron Lett 2008;49:5515–8.
[43] Tutar A, Erenler R, Biellmann JF. Synthesis of 8-substituted 4, 4-difluoro-4-bora-3a,4a-diaza-s-indacene Dyes (BODIPY). J Chem Soc Pak 2013;35:1197–201.
[44] Nagata Y, Hynková K, Damborský J, Takagi M. Construction and characterization of histidine-tagged haloalkane dehalogenase (LinB) of a new substrate class from a γ-hexachlorocyclohexane-Degrading Bacterium, *Sphingomonas paucimobilis* UT26. Protein Expr Purif 1999;17:299–304.

[45] Johnson KA, Simpson ZB, Blom T. Global kinetic explorer: a new computer program for dynamic simulation and fitting of kinetic data. Anal Biochem 2009;387:20–9.

[46] Johnson KA, Simpson ZB, Blom T. FitSpace explorer: an algorithm to evaluate multidimensional parameter space in fitting kinetic data. Anal Biochem 2009;387:30–41.